2018

Integrated zircon U-Pb-O-Hf and whole-rock Sm-Nd studies of paleozoic amphibolites in the Chencai area of the Cathaysia Block, South China

Lei Zhao
Chinese Academy Of Sciences, University of Wollongong, zlei@uow.edu.au

Bo Liu
Chinese Academy Of Sciences, University of Chinese Academy of Sciences

Allen Phillip Nutman
University of Wollongong, anutman@uow.edu.au

Mingguo Zhai
Chinese Academy Of Sciences, University of Chinese Academy of Sciences

Xiwen Zhou
Chinese Academy of Geological Sciences

See next page for additional authors

Publication Details

Zhao, L., Liu, B., Nutman, A. P., Zhai, M., Zhou, X. & Cui, X. (2018). Integrated zircon U-Pb-O-Hf and whole-rock Sm-Nd studies of paleozoic amphibolites in the Chencai area of the Cathaysia Block, South China. The Journal of Geology, 126 (6), 621-637.

Integrated zircon U-Pb-O-Hf and whole-rock Sm-Nd studies of paleozoic amphibolites in the Chencai area of the Cathaysia Block, South China

Abstract

The present metamorphic crystalline basement of the South China Block was formed largely as a result of the early Paleozoic (~460-410 Ma) orogeny, which affected large areas of this continental block. Paleozoic metamafic rocks (garnet amphibolites) with typical normal mid-ocean ridge basalt chemical compositions were recently identified from an uplifted lower-crustal rock assemblage in the Chencai area of the Cathaysia Block. This article focuses on the first integrated studies of secondary-ion mass spectroscopy (SIMS) zircon U-Pb dating and zircon Lu-Hf-O and whole-rock Sm-Nd isotopic analyses on these metamafic rocks, for the purpose of better constraining the ancient geodynamic processes of this orogeny. The SIMS zircon U-Pb dating results show that these mafic rocks underwent high-grade metamorphism at ~427 Ma, within the time span of Paleozoic orogeny. Most zircon Lu-Hf and O isotopic results display relatively uniform compositions, with $\delta^{18}O$ values scattering around +9‰ and the calculated $\varepsilon_{Hf}(t)$ values of most metamorphic zircons ranging from +9.8 to +15.1. The $^{143}Nd/^{144}Nd$ and $^{147}Sm/^{144}Nd$ ratios of the three samples are 0.513075-0.513103 and 0.20508-0.205832, respectively. The $\varepsilon_{Nd}(t)$ values are high positive, ranging from +8.05 to +8.63. These ratios resemble those of basaltic rocks newly derived from a depleted-mantle source. Zircon Hf model ages are ~540 Ma, older than the previous result of ~496 Ma, suggesting that these newly formed crustal materials were likely extracted from the depleted-mantle source during the early Paleozoic. It is thus inferred from such isotopic characteristics, as well as previously published data of the metamafic rocks, that the previous notion-that a deep lithospheric fracture reaching asthenospheric mantle was absent from the Early Paleozoic South China Orogen-should be reconsidered.

Publication Details

Zhao, L., Liu, B., Nutman, A. P., Zhai, M., Zhou, X. & Cui, X. (2018). Integrated zircon U-Pb-O-Hf and whole-rock Sm-Nd studies of paleozoic amphibolites in the Chencai area of the Cathaysia Block, South China. The Journal of Geology, 126 (6), 621-637.

Authors

Lei Zhao, Bo Liu, Allen Phillip Nutman, Mingguo Zhai, Xiwen Zhou, and Xiahong Cui

Integrated Zircon U-Pb-O-Hf and Whole-Rock Sm-Nd Studies of Paleozoic Amphibolites in the Chencai Area of the Cathaysia Block, South China

Lei Zhao,[1,2,*] *Bo Liu,*[1,3] *Allen P. Nutman,*[2] *Mingguo Zhai,*[1,4] *Xiwen Zhou,*[5] *and Xiahong Cui*[1,3]

1. State Key Laboratory of Lithospheric Evolution, Institute of Geology and Geophysics, Chinese Academy of Sciences, Beijing 100029, China; 2. GeoQuEST Research Centre, School of Earth and Environmental Sciences, University of Wollongong, Wollongong, New South Wales 2522, Australia; 3. University of Chinese Academy of Sciences, Beijing 100049, China; 4. Key Laboratory of Computational Geodynamics, University of Chinese Academy of Sciences, Beijing 100049, China; 5. Institute of Geology, Chinese Academy of Geological Sciences, Beijing 100037, China

ABSTRACT

The present metamorphic crystalline basement of the South China Block was formed largely as a result of the early Paleozoic (~460–410 Ma) orogeny, which affected large areas of this continental block. Paleozoic metamafic rocks (garnet amphibolites) with typical normal mid-ocean ridge basalt chemical compositions were recently identified from an uplifted lower-crustal rock assemblage in the Chencai area of the Cathaysia Block. This article focuses on the first integrated studies of secondary-ion mass spectroscopy (SIMS) zircon U-Pb dating and zircon Lu-Hf-O and whole-rock Sm-Nd isotopic analyses on these metamafic rocks, for the purpose of better constraining the ancient geodynamic processes of this orogeny. The SIMS zircon U-Pb dating results show that these mafic rocks underwent high-grade metamorphism at ~427 Ma, within the time span of Paleozoic orogeny. Most zircon Lu-Hf and O isotopic results display relatively uniform compositions, with $\delta^{18}O$ values scattering around +9‰ and the calculated $\varepsilon_{Hf}(t)$ values of most metamorphic zircons ranging from +9.8 to +15.1. The $^{143}Nd/^{144}Nd$ and $^{147}Sm/^{144}Nd$ ratios of the three samples are 0.513075–0.513103 and 0.20508–0.205832, respectively. The $\varepsilon_{Nd}(t)$ values are high positive, ranging from +8.05 to +8.63. These ratios resemble those of basaltic rocks newly derived from a depleted-mantle source. Zircon Hf model ages are ~540 Ma, older than the previous result of ~496 Ma, suggesting that these newly formed crustal materials were likely extracted from the depleted-mantle source during the early Paleozoic. It is thus inferred from such isotopic characteristics, as well as previously published data of the metamafic rocks, that the previous notion—that a deep lithospheric fracture reaching asthenospheric mantle was absent from the Early Paleozoic South China Orogen—should be reconsidered.

Online enhancements: appendix and supplemental tables.

Introduction

The South China Block (SCB), which occupies the whole of South China in the southeastern Eurasian continent, is a continental block with a rather complex tectonic evolutionary history. To the north, the SCB is bounded by the Qinling-Dabie-Sulu high-pressure–ultrahigh-pressure metamorphic belt, which is the subduction and continental-collision zone between the SCB and the North China Craton. Its western-northwestern and the southwestern boundaries are usually considered to be the Longmenshan fault and the Song-Ma fault, respectively (fig. 1). The SCB is generally considered to consist of three tectonic units, namely, the Yangtze Block in the northwest, the Cathaysia Block in the southeast, and the Jiangnan belt in the middle, which welded the former two together during the Neoproterozoic (fig. 1; Shu et al. 1994; Charvet et al. 1996; X.-H. Li et al. 1997, 2009*a*; Z.-X. Li et al. 2002; Cawood et al. 2013; Zhang et al. 2013*b*; Xu et al. 2014; Zhao 2014). Even though

Manuscript received November 7, 2017; accepted July 20, 2018; electronically published September 14, 2018.

* Author for correspondence; email: zhaolei_zl@yeah.net.

[The Journal of Geology, 2018, volume 126, p. 621–637] 0022-1376/2018/12606-0004$15.00. DOI: 10.1086/699927

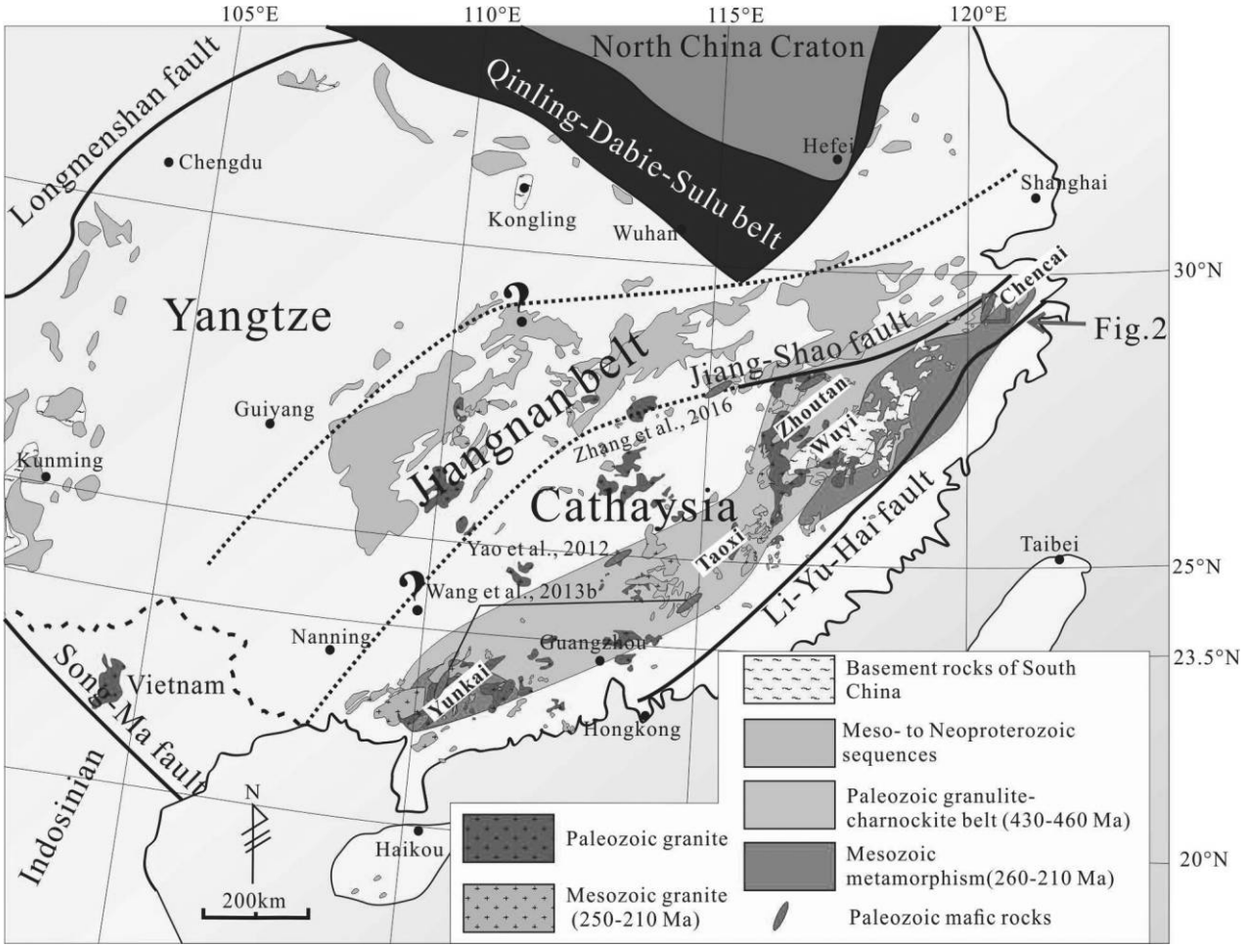

Figure 1. Simplified geological map of the South China Block, showing locations of recently reported Paleozoic mafic rocks in the Cathaysia Block. The question marks show the undefined boundaries between terranes. This map is modified after Zhao et al. (2015*c*, 2017). A color version of this figure is available online.

significant controversies still exist as to exactly when and how the amalgamation occurred (Wang et al. 2008, 2012*a*, 2014*b*; X.-H. Li et al. 2009*a*; Charvet 2013; C.-L. Zhang et al. 2013*a*; Zhao 2014; Y. Zhang et al. 2015*b*; L. Li et al. 2016; Yao et al. 2016; Zhang and Wang 2016; Zhang 2017), it is almost undeniable that the SCB achieved more than 90% of its present-day crustal materials by the late Neoproterozoic, as shown by Sm-Nd and Lu-Hf isotopic data of rocks with various zircon U-Pb ages (Jahn et al. 1990; Chen et al. 1991; Li and McCulloch 1996; Mao et al. 2011; Li et al. 2014). Besides the Neoproterozoic crustal formation event, there are three more tectonothermal events that strongly influenced the SCB: early Paleozoic, early Mesozoic, and late Mesozoic orogenies (Wong 1929; Cui and Li 1983; Ren et al. 1986; Yin et al. 1999; Xing et al. 2010, 2014; Shu 2012; Wang et al. 2013*a*; Zhang et al. 2013*b*; Ren and Li 2016). As a result of these multiple tectonothermal events, the boundaries between the three tectonic units are quite ambiguous, except the Jiang-Shao fault, which is widely believed to demarcate the Jiangnan belt and the Cathaysia Block (fig. 1).

The early Paleozoic South China orogeny (Middle Ordovician to Early Devonian, also known as the Wuyi-Yunkai orogeny) is an important tectonothermal event that shaped the present-day crystalline basement of vast areas of the SCB, involving most of the Cathaysia Block and the southeastern Yangtze Block (Huang 1941, 1960; Ren 1964; Guo et al. 1989; Ren and Chen 1989; Wang et al. 2010, 2012*b*, 2013*a*; Shu 2012; Zhang et al. 2013*b*; Shu et al. 2014). This orogeny was originally identified on the basis of a widespread unconformity between the Devonian sedimentary rocks and pre-Devonian metamorphic basement (see the reviews by Shu 2012, Wang et al. 2012*b*, and Shu et al. 2014). Yang et al. (1995), Zhao et al. (1996), Wu et al. (1998), and He

et al. (2000) presented several lines of evidence arguing for the existence of Paleozoic oceanic crust, and they interpreted this orogeny to indicate continent or microcontinent amalgamation during the Paleozoic. Tectonic models such as "soft collision," "polycyclic suturing," and "multiple terrane accretion" were also proposed to address the absence of contemporaneous high-pressure metamorphic rocks, which are usually found in small volumes in collisional and accretionary plate boundaries (Guo et al. 1984; Jahn et al. 1990; Ren et al. 1999; Yin et al. 1999). Many other studies suggested that oceanic rocks are absent from the Paleozoic SCB (Ren et al. 1986; Li 2000; Faure et al. 2009). Because of the absence of Paleozoic ophiolites and high-pressure metamorphism, as well as the continuous Paleozoic sedimentation across vast areas of South China (Chen et al. 2010, 2012; Shu 2012; Shu et al. 2014), the early Paleozoic orogen has been widely regarded as an intraplate orogen (Ren et al. 1986; Ren and Chen 1989; Lin et al. 2008; Faure et al. 2009; Z.-X. Li et al. 2010*c*; S. Li et al. 2012; Shu 2012; Wang et al. 2012*b*; Shu et al. 2014). Deep lithospheric fracture reaching asthenospheric mantle was further inferred by many of the above researchers to be absent from the early Paleozoic orogen.

Mafic-ultramafic rocks, which are critical for unraveling the geodynamic processes during Paleozoic orogeny, have been reported from several places in the Cathaysia Block (fig. 1), and nearly all of these rocks were reported to be derived from enriched lithospheric mantle sources (Yao et al. 2012; Wang et al. 2013*b*; Zhang et al. 2016; Zhao et al. 2015*b*). Wang et al. (2014*a*) and Chen et al. (2015) reported the Paleozoic garnet amphibolites from the Longyou area (along the Jiang-Shao fault), and they interpreted them to be retrograde eclogite formed through Paleozoic plate subduction and collision, which was challenged by other studies (Wang et al. 2016, 2017). Besides the amphibolites in the Longyou area, Paleozoic granulite facies rocks have also been reported in two other places along the Jiang-Shao fault, namely, the Zhoutan and Chencai areas (fig. 1; Yu et al. 2014; Zhao et al. 2015*b*, 2016). Among the suite of mafic to ultramafic rocks, the garnet amphibolites show chemical characteristics similar to those of normal mid-ocean ridge basalt (N-MORB), with flat rare earth element (REE) patterns (Zhao et al. 2015*b*), and this is the first discovery of Paleozoic mafic rocks with such chemical compositions. In this study, we present integrated studies of field occurrences, petrographic observations, zircon U-Pb-O-Hf data, and whole-rock Sm-Nd isotopic characteristics of these garnet amphibolites. These results coherently support that their protolith represents Paleozoic juvenile crustal materials derived from a depleted-mantle source.

Geological Background and Samples

Two different areas, one mainly exhibiting early Paleozoic and the other mainly showing Mesozoic metamorphic overprinting, have been identified from the Cathaysia Block (Zhao et al. 2015*c*; fig. 1). The Chencai area, located in the northeastern Cathaysia Block, is well within the Paleozoic belt, representing the northeastern extension of the Early Paleozoic South China Orogen. Rocks that extensively outcrop in this area were assigned to the Chencai Group (fig. 2), and they were previously divided into four formations: the Daojiuwan, Xiahetu, Xiawuzhai, and Xu'an Formations (Kong et al. 1995). The Daojiuwan Formation is dominated by interlayered amphibolite, biotite gneiss, and quartzite. The Xiahetu Formation is mainly composed of interlayered amphibolite, marble, and feldspathic leptynite. The Xiawuzhai Formation is dominated by interlayered garnet pyroxene amphibolite and biotite gneiss. Rocks of the Xu'an Formation are mainly sillimanite garnet biotite gneiss containing graphite gneiss. The protolith associations have been interpreted to be a tectonically disrupted flysch formation, belonging to a sequence of aluminum-rich sedimentary rocks and volcanic rocks (Kong et al. 1995). This division was actually based on rock assemblages and characteristics shown by rocks of different regions, rather than on the primary stratigraphic characteristics of a defined sedimentary sequence. Instead, strong ductile deformation and anatexis have eliminated all primary sedimentary textures (fig. 3*A*, 3*B*). Typical metamorphic minerals, such as garnet, sillimanite, graphite, and biotite, are pervasive in rocks of all four "formations." Geochronological studies show that these rocks underwent high-grade metamorphism and extensive anatexis during 420–450 Ma (fig. 3*A*, 3*B*; Zhao et al. 2016; Li et al. 2018). Detrital zircons of these metasedimentary rocks are dominated by Neoproterozoic populations with an age range of 780–830 Ma (Yao et al. 2014; Zhao et al. 2016).

As shown in figure 2, some mafic-ultramafic rocks also occur in the Chencai region, besides the Chencai Group metasedimentary rocks. These mafic-ultramafic rocks, as well as the Chencai Group metasedimentary rocks, used to be regarded as Neoproterozoic mélange related to the Neoproterozoic amalgamation between the Yangtze and Cathaysia Blocks at the expense of a Neoproterozoic ocean. Zhao et al. (2015*b*) proved that these mafic-ultramafic rocks were actually formed during the early Paleozoic, rather than the Neoproterozoic. These rocks occurring in the Chencai region are considered by some researchers to represent a Paleozoic convergent plate boundary accretionary complex developed dur-

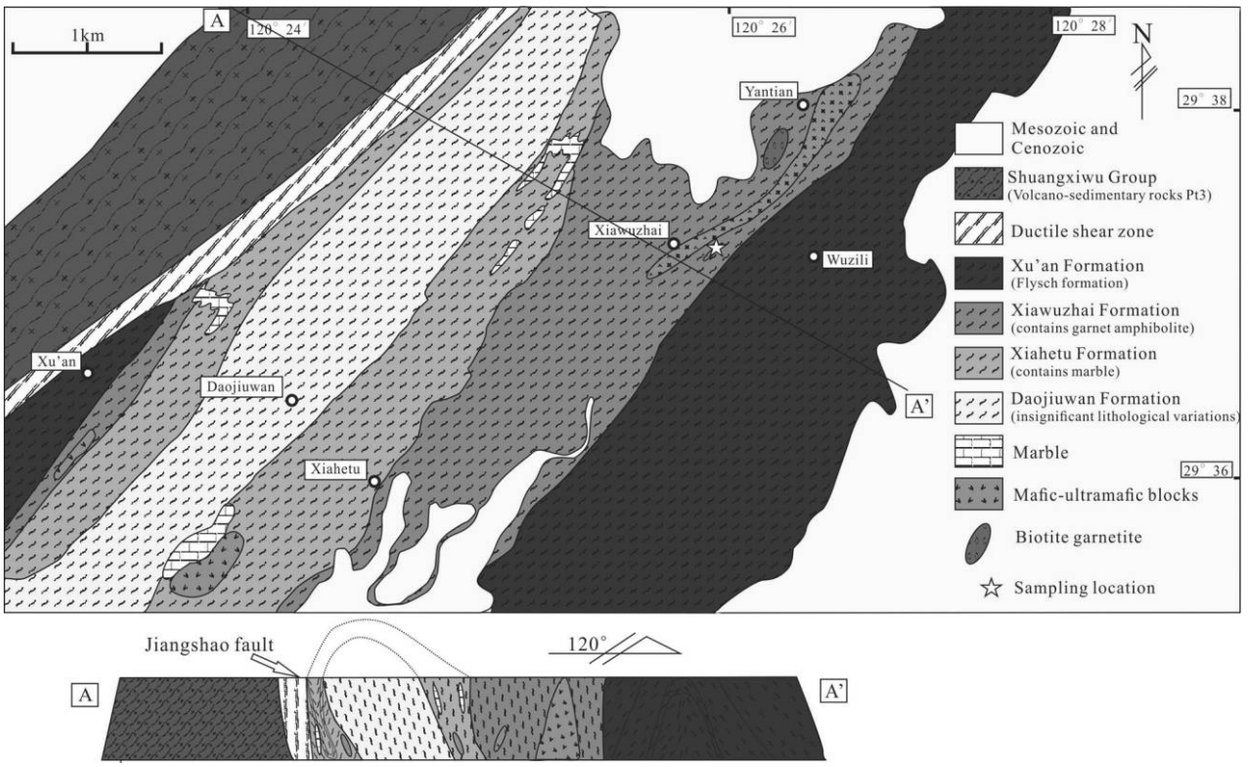

Figure 2. Simplified geological map of the Chencai area, showing the location of the studied metamafic rocks of this article. This map is modified after Zhao et al. (2015*b*, 2016) and Kong et al. (1995). A color version of this figure is available online.

ing the Early Paleozoic South China Orogen (Wang et al. 2014*a*). In that case, the Chencai Group contains allochthonous bodies of rocks derived from an active convergent plate boundary, with possible intercalations of rocks from the subducted plate. There are also other interpretations that this rock association might represent the uplifted middle- to lower-crustal component during the Paleozoic orogeny (Z.-X. Li et al. 2010*c*; J. Li et al. 2017). These mafic-ultramafic rocks occur as lenses, deformed small plutons, and dismembered blocks within the metasedimentary rocks (anatectic migmatites; fig. 3*C*–3*F*). Most of these mafic-ultramafic rocks underwent amphibolite to granulite facies metamorphism (Zhao et al. 2016). Geochemical and isotopic characteristics of part of the mafic-ultramafic rocks, together with the metamorphism of the Chencai region, led Zhao et al. (2015*b*) to propose that these rocks are actually uplifted lower-crust components and likely represent orogenic root associations formed during the early Paleozoic. To the northwestern part of the Chencai area is the Jiang-Shao fault (ductile shear zone; fig. 1). The Neoproterozoic Shuangxiwu Group, of which most of the rocks underwent only greenschist facies metamorphism, lies to the other side of the Jiang-Shao fault (fig. 2).

All the samples in this study were collected from the Chencai area, and they occur as lenses or dismembered blocks in anatectic migmatites of the Chencai Group. Intrusive thin leucosome veins derived from anatectic metasedimentary rocks can be seen on most outcrops of garnet amphibolite (fig. 3). The three samples (15CC02-2, 15CC02-3, and CC13-05) studied all have the same mineral assemblage of garnet + amphibole + plagioclase + biotite + ilmenite, and some quartz where many garnet grains are present. All the primary magmatic textures have been replaced by amphibolite facies metamorphic textures (fig. 4).

Analytical Techniques

Standard heavy-liquid and magnetic techniques were used in zircon grain separation, after the samples were crushed. Zircon grains were then handpicked under a binocular microscope. The selected grains, together with zircon standards (see detailed descriptions below), were then cast in 25-mm epoxy disks and then were ground and polished to expose midsections through the grains for cathodoluminescence (CL) imaging, U-Pb dating, and O and Lu-Hf

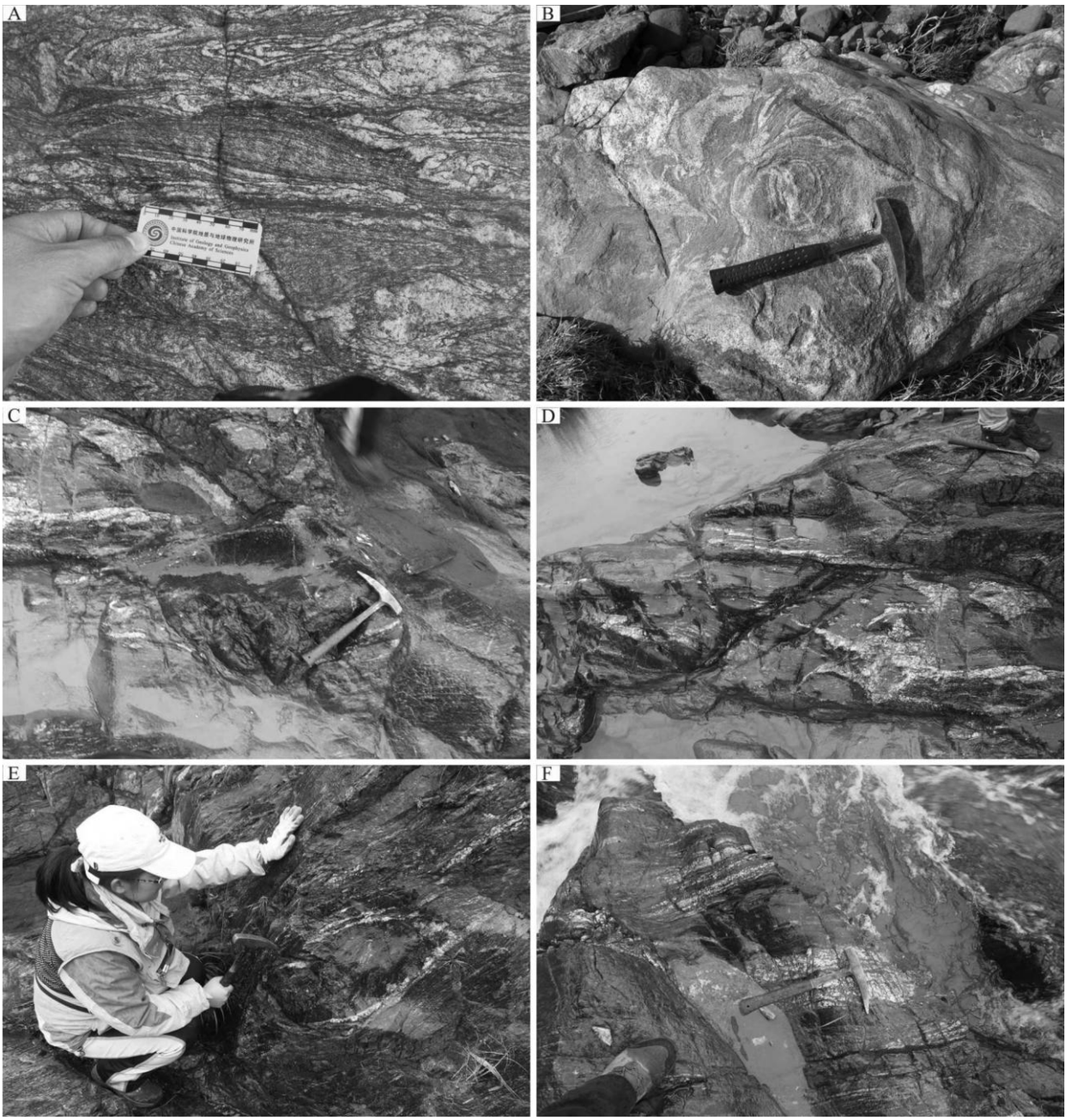

Figure 3. Field photos of the anatectic migmatites belonging to the Chencai Group (*A*, *B*) and the metamafic rocks occurring as dismembered blocks or lenses (*C–F*). A color version of this figure is available online.

isotope analyses. The internal zoning was examined with a CL detector (Garton Mono CL3+) installed on a Quanta 200F environmental SEM, with a 2-min scanning time under conditions of 15 kV and 120 nA, at the Institute of Geology, Chinese Academy of Geological Sciences.

Secondary-ion mass spectrometry (SIMS) zircon U-Pb dating was also conducted at the Institute of Geology and Geophysics, Chinese Academy of Sciences (IGGCAS), with a CAMECA IMS 1280 SIMS (spectrometer). Detailed analytical procedures can be found in X.-H. Li et al. (2009*b*) and Q.-L. Li et al. (2010*a*). During analysis, the O_2^- primary ion beam was accelerated at 13 kV, and the intensity was ~10 nA. The ellipsoidal spot is about 20 μm × 30 μm in size. Oxygen flooding was used to increase the O_2 pressure to ca. 5×10^{-6} torr in the sample chamber, enhancing Pb^+ sensitivity by a factor of >2, to a value

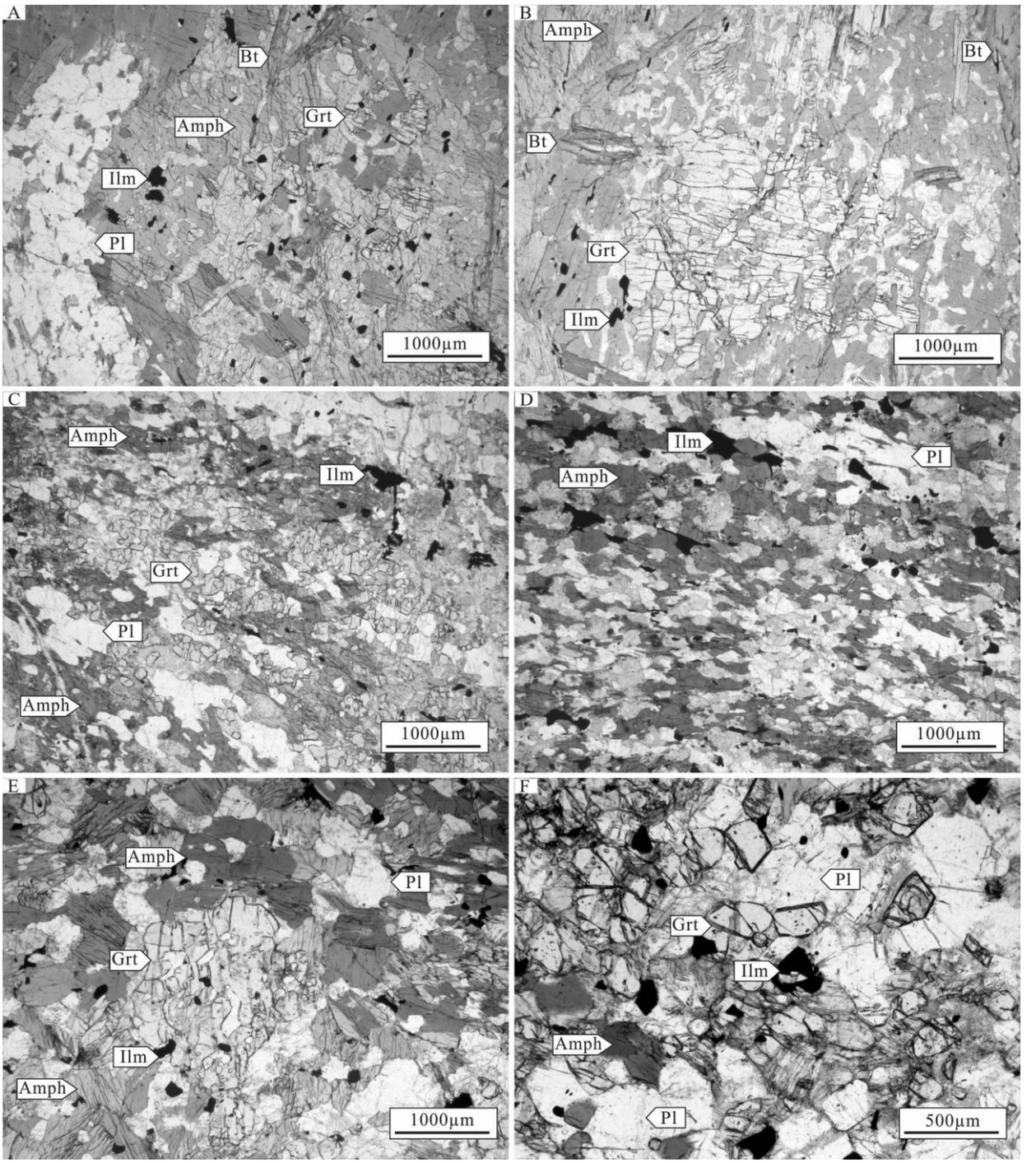

Figure 4. Photomicrographs showing the representative mineral assemblages and metamorphic textures of the three garnet amphibolite samples: 15CC02-2 (*A*, *B*), 15CC02-3 (*C*, *D*), and CC15-03 (*E*, *F*). Amph = amphibolite; Bt = biotite; Grt = garnet; Ilm = ilmenite; Pl = plagioclase. A color version of this figure is available online.

of ca. 25–28 counts per second (cps)/nA/ppm for zircon (X.-H. Li et al. 2009*b*). Zircon standard Plešovice, with a known age of 337 Ma (Sláma et al. 2008), was used to calibrate the measured Pb/U ratios. A long-term uncertainty of 1.5% (1 relative SD) for $^{206}Pb/^{238}U$ measurements of the Plešovice standard was propagated to the unknowns, even though the measured $^{206}Pb/^{238}U$ error in a specific session is generally around 1% (1 relative SD) or less (Q.-L. Li et al. 2010*a*). The measured Pb isotopic compositions were cor-

rected for common Pb with nonradiogenic ^{204}Pb. An average present-day crustal Pb composition (Stacey and Kramers 1975) was used for common Pb, on the assumption that the common Pb was largely due to surface contamination introduced during sample preparation. The data were assessed with the ISOPLOT program (Ludwig 2012). Twelve analyzed standard Qinghu zircon spots, as unknowns, gave a weighted mean $^{206}Pb/^{238}U$ age of 159.9 ± 1.9 Ma (MSWD = 0.87). After analytical errors are taken into consideration, this age is consistent with the recommended $^{206}Pb/^{238}U$ age of 159.9 ± 0.2 Ma (2 SE; X.-H. Li et al. 2009*b*).

The zircon oxygen isotopic compositions were also analyzed with the CAMECA IMS 1280 SIMS at IGGCAS. Detailed analytical procedures were similar to those described by Li et al. (2010*b*). The Cs^+ primary-ion beam was accelerated at 10 kv, with an intensity of ~2 nA. The spot size was ~20 μm in diameter. A normal-incidence electron flood gun was used to compensate for sample charging during analysis. Oxygen isotopes were measured in multicollection mode on two off-axis Faraday cups, with mass resolution of ~2500 (slit 2). The intensity of ^{16}O was typically no less than 1×10^9 cps. Each analysis took less than 4 min, consisting of presputtering (ca. 60 s), automatic beam centering (ca. 60 s), and integration of oxygen isotopes (20 cycles × 4 s). The instrumental mass fractionation factor (IMF) was corrected with zircon standard Penglai, with a $\delta^{18}O$ (Vienna standard mean ocean water) value of 5.3‰ ± 0.1‰ (2σ; Li et al. 2010*b*). The standard data were collected regularly throughout the analytical session as the IMF drifted with time (standard data are presented in table S1; tables A1–A4 and S1 are available online). The Qinghu zircon standard was measured as an unknown and yielded a standard deviation of 0.4‰ (2σ), which was used for least uncertainty for individual analysis. Uncertainty on individual analysis was usually better than 0.2‰–0.3‰ (2σ).

Zircon Hf isotope analyses were also carried out in the State Key Laboratory of Lithospheric Evolution at IGGCAS, with a Neptune multicollector (MC-)ICPMS. A 40–63-μm spot size was applied during ablation with a 193-nm laser, with a repetition rate of 10 Hz in most cases. Detailed descriptions of the instrument and analytical procedures are similar to those in Wu et al. (2006). The domains of zircon grains chosen for Hf isotopic analyses were the same as those for the O isotope analysis and U-Pb dating. Two zircon standards, GJ and Mud Tank, whose U-Pb ages and Hf isotope compositions are quite uniform and well documented (Woodhead and Hergt 2005; Zeh et al. 2007; Xie et al. 2008), were used to monitor the stability of the instrument during analyses. In the analytical sessions reported here, the weighted $^{176}Hf/^{177}Hf(c)$ value of GJ was 0.2820032 ± 0.0000041 (n = 26, MSWD = 0.84), and the weighted $^{176}Hf/^{177}Hf(c)$ of Mud Tank was 0.282495 ± 0.000005 (n = 10, MSWD = 0.86; "c" denotes "corrected"), which, after taking the analytical errors into consideration, are consistent with the values recommended previously (Woodhead and Hergt 2005; Zeh et al. 2007; Xie et al. 2008). On the basis of depleted-mantle and chondrite sources, model ages ($T_{DM}(Hf)$) and $\varepsilon_{Hf}(t)$ of zircon grains were calculated. The values of $^{176}Hf/^{177}Hf$ and $^{176}Lu/^{177}Hf$ are 0.28325 and 0.0384 for modeled depleted mantle (Griffin et al. 2002) and 0.282772 and 0.0332 for chondrite, respectively (Blichert-Toft and Albarède 1997). The decay constant of ^{176}Lu adopted in this article is 1.867×10^{-11} per year (Söderlund et al. 2004).

Whole-rock Sm-Nd isotopic analyses were conducted at IGGCAS. Detailed descriptions of instruments involved and analytical procedures are presented in Yang et al. (2010) and Li et al. (2011*a*, 2011*b*). As mentioned above, the amphibolites were intruded by thin anatectic veins during regional metamorphism (fig. 3). During preparation of sample powders for Sm-Nd isotope analyses, these veins were all removed after the samples were broken into small pieces. Very fine-grained whole-rock powders for Nd isotopic analyses were dissolved in Savillex Teflon screw-top capsules after being spiked with mixed ^{149}Sm-^{150}Nd tracers before $HF+HNO_3+HClO_4$ dissolution. The classical two-step ion exchange chromatographic method was used for Sm and Nd separation. The samples were then measured with a Finnigan MAT262 MC thermal ionization mass spectrometer (MC-TIMS). The blank during the whole procedure was lower than 100 pg. The isotopic ratios were corrected for mass fractionation by normalizing to $^{146}Nd/^{144}Nd = 0.7219$. The international standard sample JNdi-1 was employed to evaluate instrument stability during the period of data collection. The measured values for JNdi-1 were $^{143}Nd/^{144}Nd$ = 0.512118 ± 0.000007 (n = 3, MSWD = 0.38). The USGS reference material BCR-2 was measured to monitor the accuracy of the analytical procedures, with the following result: $^{143}Nd/^{144}Nd$ = 0.512624 ± 0.000012 (n = 1), which is consistent with the suggested value of BCR-2 yielded by TIMS and MC-ICPMS techniques (Yang et al. 2010; Li et al. 2011*a*, 2011*b*).

Results

Zircon U-Pb Dating Results. Most zircon grains from the three garnet amphibolite samples show characteristics similar to those shown by the CL images

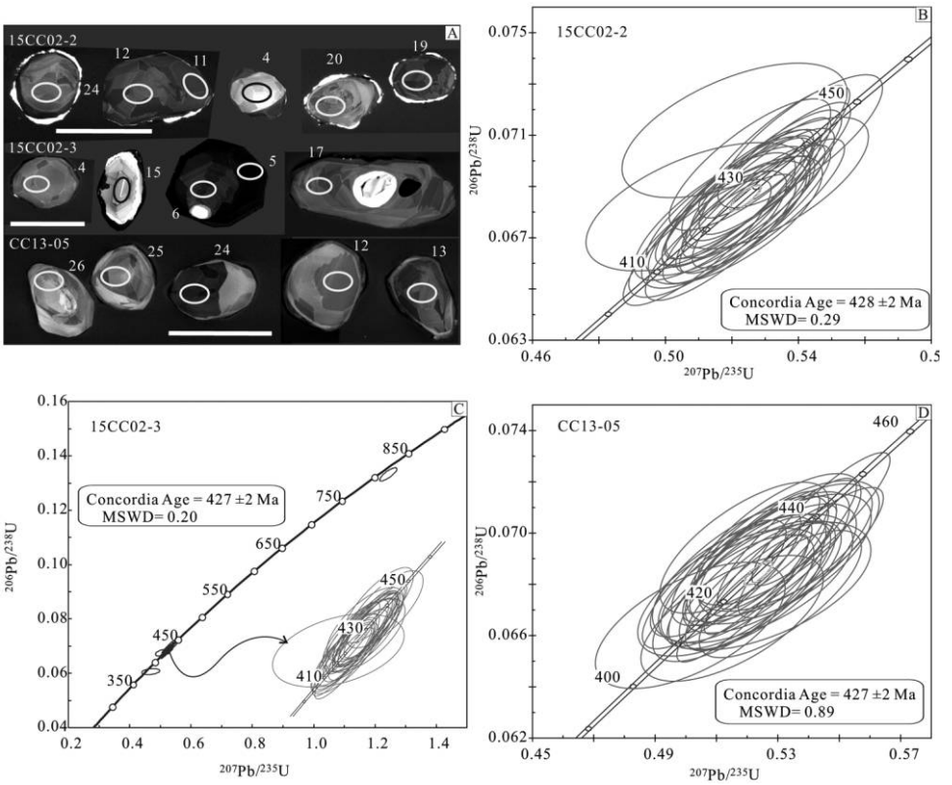

Figure 5. *A*, Cathodoluminescence images of representative zircon grains; the scale bars are all 100 μm. *B–D*, Secondary-ion mass spectroscopy zircon U-Pb results. A color version of this figure is available online.

(fig. 5). These zircons are mostly round or elliptical, exhibiting low aspect ratios (mostly between 1:1 and 3:1) and displaying low-luminescence characteristics. Some of the grains have very high-luminescence narrow rims and dark mantles (e.g., grain 24 of 15CC02-2 in fig. 5*A*) that are too narrow for dating. Several grains from these three samples show core-rim structures with cores exhibiting higher luminescence than rims, and some cores (only in sample 15CC02-3) display oscillatory zoning patterns. Most zircon grains and some zircon cores show sector zoning or fir-tree zoning patterns or lack any zoning (fig. 5*A*).

A total of 86 spots from the three samples (15CC02-2, 15CC02-3, and CC13-05) were analyzed for U-Pb ages. The results are presented in table A1 and figure 5. Of the 28 spots analyzed on zircons from 15CC02-2, the $^{206}Pb/^{238}U$ ages range from 416 to 443 Ma, and related Th/U ratios range from 0.05 to 0.13 (mostly <0.1). Most of the analyzed results show high concordance (>90%), and the concordia age of this sample is 428 ± 2 Ma (MSWD = 0.29). Several analyses were done on zircon cores, and most of them exhibit $^{206}Pb/^{238}U$ ages similar to those from the analyses of other zircon sites, such as the zircon grain with two spots (25 [rim] and 26 [core]). However, exceptions do exist. For example, the $^{206}Pb/^{238}U$ age of spot 12 is 443 ± 6 Ma, while that of spot 11, the rim part of the same zircon grain, is 422 ± 6 Ma, younger than that of spot 12. Of the 29 spots analyzed on zircons from 15CC02-3, the $^{206}Pb/^{238}U$ ages range from 379 to 806 Ma. The spot with the young $^{206}Pb/^{238}U$ age of 379 Ma is discordant (−17%). As to the old $^{206}Pb/^{238}U$ age of 806 Ma, this age result was given by an oscillatory-zoned zircon core, and the Th/U ratio of this spot is 0.69 (spot 15; fig. 5*A*). All the other spots gave $^{206}Pb/^{238}U$ ages of 416–440 Ma, with Th/U ratios ranging from 0.01 to 0.17 (mostly <0.1; table A1). Some of these spots have relatively older ages of 435–440 Ma and/or high Th/U ratios (>0.15), and they are all zircon cores, such as spots 6 ($^{206}Pb/^{238}U$ age = 431 Ma, Th/U = 0.17), 13 ($^{206}Pb/^{238}U$ age = 440 Ma, Th/U = 0.04), and 23 ($^{206}Pb/^{238}U$ age = 438 Ma, Th/U = 0.02). All other core spots exhibit $^{206}Pb/^{238}U$ ages indistinguishable from those of zircon rims. Concordant ages of this sample give a weighted mean $^{206}Pb/^{238}U$ age of 427 ± 2 Ma (MSWD = 0.2; fig. 5*C*). Twenty-nine spots on the other garnet amphibolite sample, CC13-05, were analyzed, and their $^{206}Pb/^{238}U$ ages range from 414 to 439 Ma. Several zircon cores in this sample give ages similar to those from other analysis sites. All of the data show high concordance, and they give a weighted mean average $^{206}Pb/^{238}U$ age

of 427 ± 2 Ma (MSWD = 0.89; fig. 5*D*). Their Th/U ratios range from 0.03 to 0.13, and only two spots on cores display Th/U ratios of >0.1 (table A1).

Zircon O and Lu-Hf Isotopic Results. Zircon O isotope analyses were undertaken on all three garnet amphibolite samples, and the results are shown in table A2 and figures 6 and 7. The $\delta^{18}O$ values of 28 analyzed spots on zircons of 15CC02-2 range from 8.38‰ to 9.74‰, and they show two peaks, at 8.9‰ and 9.2‰ (fig. 6*A*). Even though most spots (including zircon cores and rims) exhibit similar $\delta^{18}O$ values, spots with the lowest $\delta^{18}O$ values are all zircon cores (e.g., spots 2 and 26; fig. 7; table A2), while spots with the highest $\delta^{18}O$ values are all zircon rims (e.g., spot 11; fig. 7; table A2). The $\delta^{18}O$ values of 29 analyzed spots on zircons of 15CC02-3 range from 8‰ to 9.33‰, and they show a peak at 9.1‰ (fig. 6*C*). Like those in sample 15CC02-2, the lowest $\delta^{18}O$ values of this sample are also given by zircon cores (e.g., spots 15 and 23; fig. 7; table A2), while the highest $\delta^{18}O$ values are given by zircon rims. The $\delta^{18}O$ values of 29 analyzed spots on zircons of CC13-05 scatter within a small range of 8.94‰–9.96‰, with a peak of 9.4‰ (fig. 6*E*).

Zircon Lu-Hf isotopic results of these three samples are presented in table A3 and figures 6–8. All the analyzed grains show low $^{176}Lu/^{177}Hf$ ratios (mostly <0.002), and most analyzed grains have $^{176}Hf/^{177}Hf$ ratios within a small range (fig. 7). During the calculation of $\varepsilon_{Hf}(t)$ values, the apparent zircon $^{206}Pb/^{238}U$ age for each zircon was used. Of the 28 analyzed spots

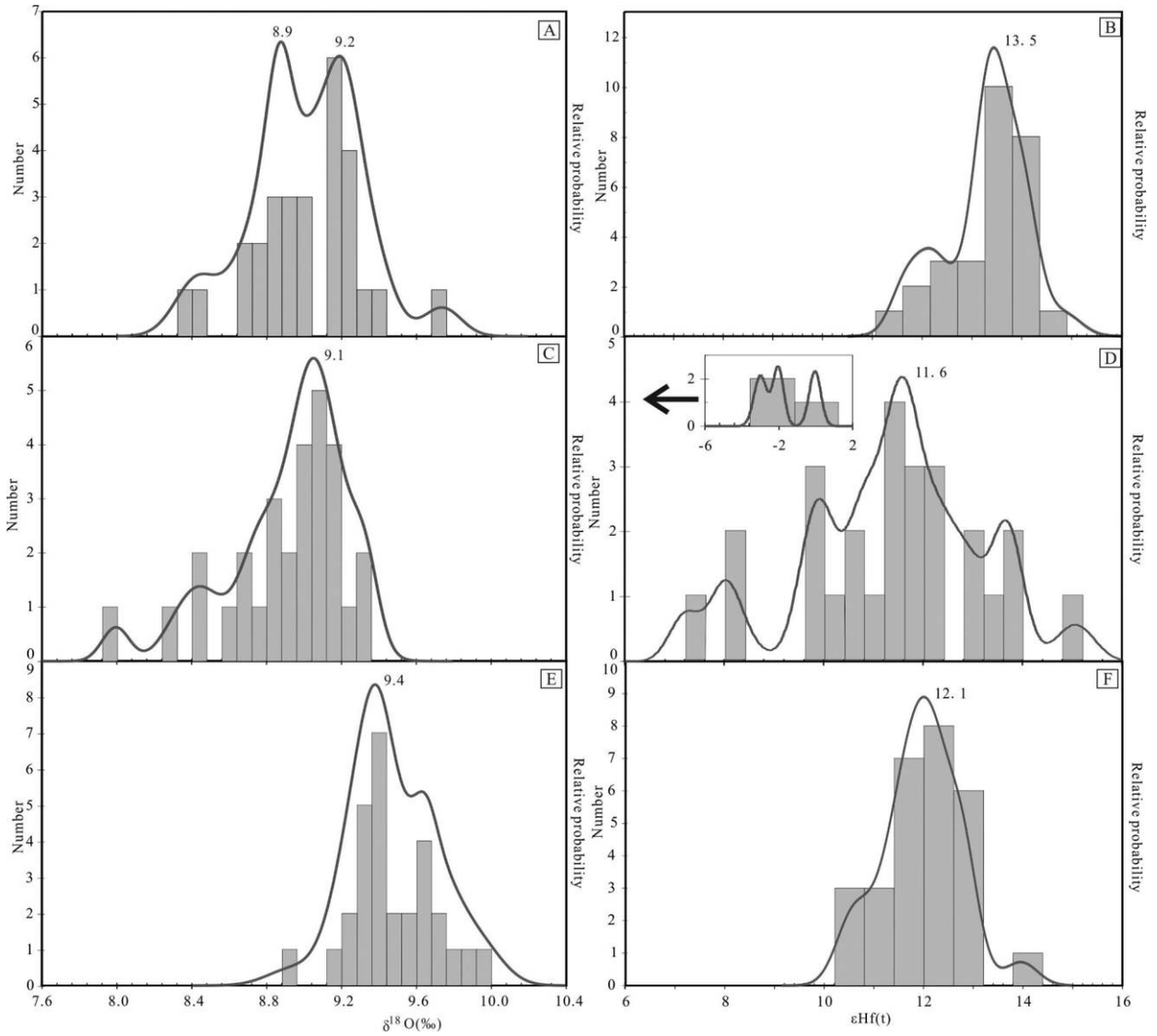

Figure 6. Secondary-ion mass spectroscopy zircon O isotope results (*A*, *C*, *E*) and $\varepsilon_{Hf}(t)$ value probability density diagrams of zircon Lu-Hf results (*B*, *D*, *F*).

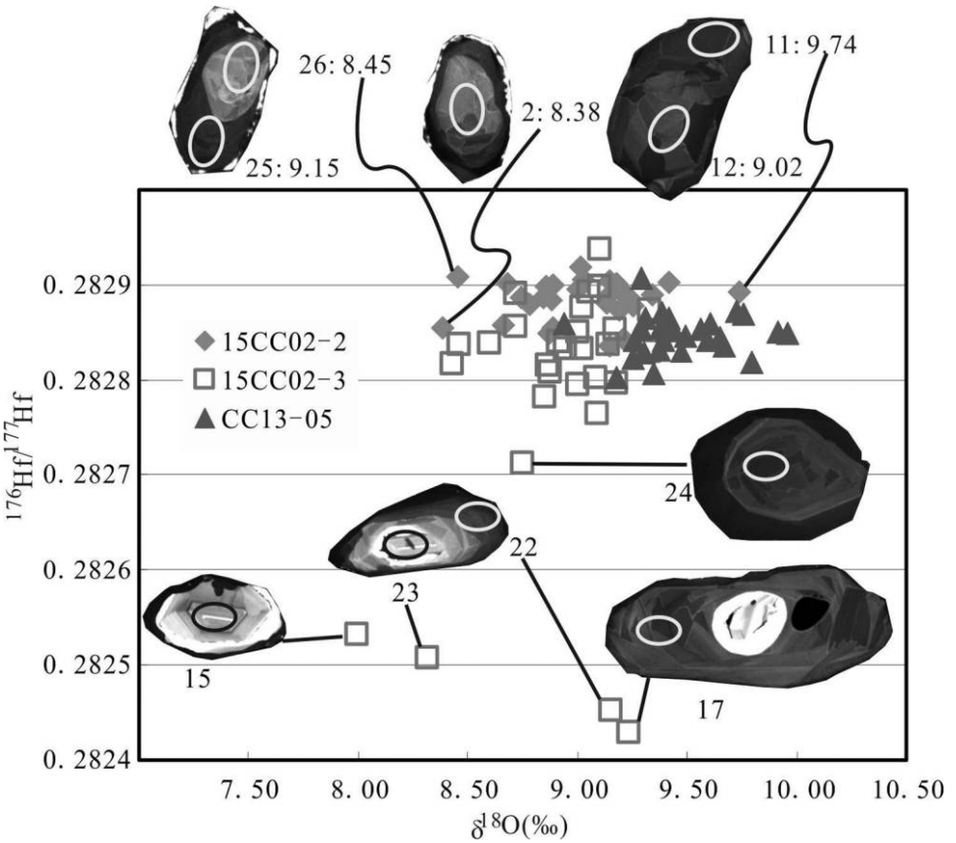

Figure 7. Zircon $^{176}Hf/^{177}Hf$ ratio versus $\delta^{18}O$ value diagram of the three metamafic samples.

on zircons from 15CC02-2, the $^{176}Hf/^{177}Hf$ ratios are 0.282836–0.282919 and the calculated $\varepsilon_{Hf}(t)$ values and model ages (T_{DM1}(Hf)) scatter within ranges of 11.6–14.88 and 463–571 Ma, respectively (table A3). The $\varepsilon_{Hf}(t)$ values show a peak at +13.5 (fig. 6*B*). A total of 29 spots on zircons from 15CC02-3 were analyzed, and these zircons have $^{176}Hf/^{177}Hf$ ratios of 0.282430–0.282937. Calculated $\varepsilon_{Hf}(t)$ values and model ages (T_{DM1}(Hf)) are −2.99 to 15.06 and 1145–439 Ma, respectively (table A3). The several grains with low $^{176}Hf/^{177}Hf$ ratios are mostly zircon cores or zircons showing textural characteristics distinct from those of other zircons (spots 15, 17, 22–24; fig. 7). The $^{176}Hf/^{177}Hf$ ratios of these grains are similar (fig. 7). All other zircon sites have $\varepsilon_{Hf}(t)$ values of 9.8–15.06 (peaking at +11.6; fig. 6*D*) and model ages (T_{DM1}(Hf)) of 439–633 Ma (table A3). The $^{176}Hf/^{177}Hf$ ratios of the 28 analyzed spots on zircons from CC13-05 scatter within a small range of 0.282802–0.282907. Their calculated $\varepsilon_{Hf}(t)$ values range from 10.47 to 13.96, and the related model ages (T_{DM1}(Hf)) range from 480 to 624 Ma (table A3).

In the $\delta^{18}O$-versus-$^{176}Hf/^{177}Hf$ diagram (fig. 7), most grains exhibit constant $^{176}Hf/^{177}Hf$ ratios but with a greater scatter in $\delta^{18}O$ values (fig. 7), which is normal for metamorphic zircons because many fluid-assisted zircon alteration processes (e.g., coupled dissolution-reprecipitation) will change O isotope compositions of zircons but will do nothing to $^{176}Hf/^{177}Hf$ ratios of zircons (Geisler et al. 2007; Zhao et al. 2015*a*). The several grains with low $^{176}Hf/^{177}Hf$ ratios from sample 15CC02-3 exhibit negative correlations between $^{176}Hf/^{177}Hf$ ratios and $\delta^{18}O$ values (fig. 7). The one core that shows oscillatory zoning and has a $^{206}Pb/^{238}U$ age of 806 Ma has the lowest $\delta^{18}O$ value. In the zircon U-Pb age–versus-$\varepsilon_{Hf}(t)$ diagram (fig. 8*A*), most of the grains plot near the depleted-mantle evolution line. The model ages (T_{DM1}(Hf)) of the three garnet amphibolite samples peak at ca. 547 Ma (fig. 8*B*).

Whole-Rock Sm-Nd Results. The major- and trace-element whole-rock compositions of these samples were reported by Zhao et al. (2015*b*). These metamafic rocks have SiO_2 contents of ~52 wt% and MgO contents of ~7 wt% and display heavy-REE enrichment ($La/Yb_N \cong 0.7$) and almost no Eu anomalies (fig. 8*D*). Sm-Nd isotopic results of the three samples are presented in table A4 and figure 8*C*, 8*E*. All three samples have high $^{147}Sm/^{144}Nd$ ratios of 0.20508–0.205832, and their $^{143}Nd/^{144}Nd$ ratios

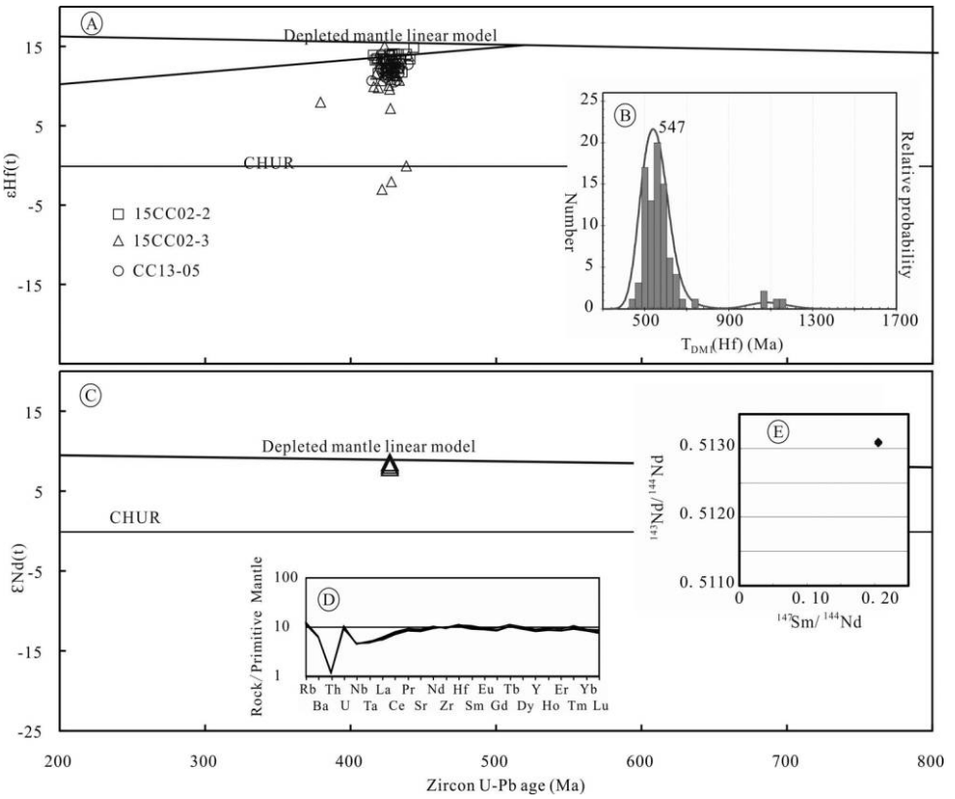

Figure 8. *A*, $\varepsilon_{Hf}(t)$ values versus zircon U-Pb ages. *B*, Probability density of zircon Hf model ages, showing a peak at ~547 Ma. *C*, $\varepsilon_{Nd}(t)$ values versus zircon U-Pb ages. *D*, Spider diagram of metamafic rocks (from Zhao et al. 2015*b*). *E*, $^{143}Nd/^{144}Nd$-versus-$^{147}Sm/^{144}Nd$ diagram, displaying whole-rock Sm-Nd compositions of metamafic rocks. CHUR = chondrite uniform reservoir.

are 0.513075–0.513103. Elemental fractionation coefficient ($f_{Sm/Nd}$) values are all near 0 (0.043–0.046; table A4). In the zircon U-Pb age–versus-$\varepsilon_{Nd}(t)$ diagram, the three samples all plot on or near the depleted-mantle evolution line (fig. 8*C*).

Discussion

Igneous and Metamorphic Geochronology. Most zircons and some zircon cores from the three garnet amphibolite samples exhibit round or ellipsoidal shapes and exhibit sector-zoning or fir-tree-zoning internal structures or lack any zoning patterns in CL images. Their Th/U ratios are mostly below 0.1. These are typical characteristics of metamorphic zircons (e.g., Vavra and Hansen 1991; Rubatto and Gebauer 1996; Rubatto et al. 1999; Vavra et al. 1999; Corfu et al. 2003). Therefore, the concordant $^{206}Pb/^{238}U$ ages of these zircons, ~427 Ma, can be considered to represent the time of Paleozoic metamorphism. Because these samples all have the same amphibolite facies mineral assemblage (amphibole + garnet + plagioclase; Miyashiro 1961; Spear 1995), this time of ~427 Ma likely represents the time of amphibolite facies metamorphism in the Chencai area. These metamorphic zircons display relatively uniform Lu-Hf but have some dispersion in O isotopic compositions.

Apart from these metamorphic zircons, two other kinds of zircons are identified according to their $^{206}Pb/^{238}U$ ages and O-Hf isotopic compositions. One group of zircons (solely consisting of structural cores) exhibit fir-tree or sector zones in CL images, typical of metamorphic zircons (e.g., Vavra and Hansen 1991; Rubatto and Gebauer 1996; Rubatto et al. 1999; Vavra et al. 1999; Corfu et al. 2003). These cores exhibit lower $\delta^{18}O$ values (~8.4‰) and/or higher $^{206}Pb/^{238}U$ ages (~440 Ma) than the above-discussed metamorphic zircons, for example, spots 2, 12, 26, and 28 in sample 15CC02-2 (fig. 7; table A2). The distinct characteristics of internal structures and Hf isotope compositions suggest that they might be the products of a different zircon formation event. Their older age of ~440 Ma (concordant $^{206}Pb/^{238}U$ ages of several zircon cores) suggests that this zir-

con formation event might correspond to an earlier metamorphic stage. These zircon cores survived the superimposed ~427 Ma metamorphism and retained their original U-Pb-O-Hf isotopic compositions. A previous study gave a metamorphic age of 436 Ma, using the zircon U-Pb laser ablation (LA)-ICPMS method (Zhao et al. 2015*b*). Besides the analytical errors that might have caused the age difference, the age of 436 Ma might be the mixed result of two episodes of metamorphism, because bigger spot sizes are needed during the LA-ICPMS analyses.

The other group of zircons is identified by distinctively low $^{176}Hf/^{177}Hf$ ratios, and they occur only in sample 15CC02-3 (fig. 7). One of them, displaying oscillatory zoning and a high Th/U ratio, gives a concordant $^{206}Pb/^{238}U$ age of 806 Ma. This zircon also shows the lowest $\delta^{18}O$ value (spot 15; fig. 7). Characteristics of this zircon indicate its magmatic origin (e.g., Vavra and Hansen 1991; Rubatto and Gebauer 1996; Rubatto et al. 1999; Vavra et al. 1999; Corfu et al. 2003). The similarity of their $^{176}Hf/^{177}Hf$ ratios suggests that the zircons of this group are primarily of the same genesis, because zircons formed from different geological processes or different sources display obviously different $^{176}Hf/^{177}Hf$ compositions (Gerdes and Zeh 2009; Zhao et al. 2015*a*). Several possibilities exist for the primary genesis of these zircons: (1) magmatic zircons crystallized from the protolith of metamafic rocks, (2) magmatic zircons entrained from the country rocks by the protolith of metamafic rocks during its emplacement, or (3) xenocrystic zircons introduced from adjacent metasedimentary rocks by the intruded anatectic veins. The first possibility is highly unlikely, for the following reasons. First, the protolith of garnet amphibolite has an undersaturated basaltic silica composition, from which magmatic zircons seldom crystallize. Second, Lu-Hf and O isotopic compositions of these grains are distinct from those of most other grains in this sample, which strongly suggests that such zircon cores are crystallized from a different chemical reservoir. According to field observations and a previously published geochronological framework of the Chencai metasedimentary rocks, we favor the third possibility. As is shown in figure 3, these mafic rocks were extensively intruded by anatectic veins originating from the Chencai metasedimentary rocks (fig. 3). Zircons with such Neoproterozoic ages and Lu-Hf isotopic compositions are abundant in these migmatitic metasedimentary rocks (Yao et al. 2014; Zhao et al. 2016; Li et al. 2018). Although less likely, the second possibility cannot be ruled out, because entrainment of zircons from country rocks during the emplacement of magmatism can easily occur. Anyway, it is safe to conclude that the Neoproterozoic age of this magmatic zircon core cannot represent the age of the protolith of these garnet amphibolites.

Zircons from the three studied samples mostly exhibit high positive $\varepsilon_{Hf}(t)$ values of ~12 (fig. 6), and the related model ages (T_{DM}(Hf)) cluster at ~547 Ma (fig. 8). The $\varepsilon_{Nd}(t)$ values calculated with whole-rock Sm-Nd isotopic results are also high positive, and the related one-stage model ages (T_{DM1}(Nd)) are Neoproterozoic to Mesoproterozoic (0.84–1.44 Ga), much older than the zircon Hf model ages. However, the Sm and Nd elemental fractionation coefficients ($f_{Sm/Nd}$) of these samples are too low (near 0), and rocks with such low $f_{Sm/Nd}$ values usually give one-stage Sm-Nd model ages older than they should be (Jahn et al. 1990). Therefore, the zircon Hf model ages of ~547 Ma, rather than the one-stage Sm-Nd model ages, can be considered to represent the approximate time of protolith magmatism derived from the depleted-mantle source. As shown by the zircon O-Hf isotopic characteristics discussed above, these metamorphic zircons experienced certain contamination from high-O and low-$^{176}Hf/^{177}Hf$ crustal materials. Therefore, only their lowest Hf model ages can be considered to represent the most appropriate estimate of protolith age, because crustal contamination would always elevate zircon Hf model ages. The study of Zhao et al. (2015*b*) gave an Hf model age of 496 Ma. We therefore propose that such an age could be a better estimate of the time of mafic magmatism.

Protolith Magma Source and Tectonic Implications. The studied garnet amphibolites have basaltic geochemical compositions, and their REE and trace-element diagrams resemble those of N-MORB (Zhao et al. 2015*b*). As discussed above, most metamorphic zircons of these three metamafic samples display relatively homogeneous Lu-Hf compositions, but with some systematic variation of the O isotopic composition from the center to the rims of the grains (fig. 7). Isotopic compositions of these metamorphic zircons can be used to trace characteristics of chemical reservoirs from which the zircons crystallized (Zhao et al. 2015*a*; Manton et al. 2017). The calculated high positive $\varepsilon_{Hf}(t)$ values and the $\varepsilon_{Hf}(t)$-versus–zircon U-Pb age diagram (fig. 8) both show that metamorphic zircons crystallized from newly formed crustal materials derived from a depleted-mantle source. Whole-rock Sm-Nd isotopic compositions of these metamafic samples are also similar to those of basalts derived from the depleted mantle (Wasserburg et al. 1981). In the $\varepsilon_{Nd}(t)$ values–versus–zircon U-Pb age diagram, these samples all plot on the depleted-mantle evolution line. Sm-Nd isotope compositions, therefore, also suggest that these garnet amphibolites were originally newly formed crustal materials from the depleted-mantle source. However, O iso-

topic compositions of these zircons ($\delta^{18}O$ values of about +9‰) are elevated over those of magmatic zircons crystallized in mantle-derived magmas (zircons equilibrated with mantle-derived melts have $\delta^{18}O$ values of ~5.3‰ ± 0.6‰; Valley et al. 1998; Valley 2003). A possible explanation for these contrasting isotopic characteristics might be that the O isotopic compositions of the fluids from which most zircons crystallized had been equilibrated with high-$\delta^{18}O$ sediments yet still retained the Lu-Hf isotopic composition of the original basalts. Zircon O isotope results show that as metamorphic zircon growth progressed, there was an overall shift in $\delta^{18}O$ from below +9 to above +9 (fig. 7). This is interpreted as reflecting the evolving fluid-phase compositions as metamorphism progressed, perhaps related to the involvement of more high-$\delta^{18}O$ components during metamorphism.

Apart from the mafic rocks of this study, which indicate an early Paleozoic depleted-mantle source, all other Paleozoic mafic-ultramafic rocks (with magmatic zircon U-Pb ages of 420–450 Ma) reported from the Cathaysia Block exhibit enriched chemical and isotopic compositions, indicating an enriched-mantle source (Yao et al. 2012; Wang et al. 2013*b*; Zhao et al. 2015*b*; Zhang et al. 2016). As described above, several different geodynamic processes have been proposed to address the petrogenesis of these rocks. Yao et al. (2012) proposed that lithospheric mantle metasomatism occurred during the Paleozoic postorogenic stage and that this process was achieved by delamination of the orogenic root, while Wang et al. (2013*b*) suggested a model in which the lithospheric mantle was metasomatized during the Neoproterozoic. For both of these models, postorogenic delamination behaved as the trigger of the partial melting of lithospheric mantle, which thus formed these mafic rocks. Zhang et al. (2015*a*, 2016) and Zhao et al. (2015*b*, 2016), however, proposed that this orogeny might have involved significant subduction (or underthrusting) and that fluids derived from subducted materials during the early Paleozoic resulted in the metasomatism and partial melting of lithospheric mantle. Although these different models have been proposed, a consensus exists among most of these researchers that deep lithospheric fracture reaching asthenospheric mantle was absent from the early Paleozoic orogenic belt (e.g., Ren et al. 1986; Ren and Chen 1989; Lin et al. 2008; Z.-X. Li et al. 2010*c*; S. Li et al. 2012; Shu 2012; Wang et al. 2012*b*, 2013*b*; Yao et al. 2012; Shu et al. 2014; Zhao et al. 2015*b*; Zhang et al. 2016). However, the metamafic rocks of this study seem to suggest a different tectonic setting for the Paleozoic orogeny of South China, if they were not allochthonous components originally formed at other continental boundaries.

Conclusions

1. The garnet amphibolites (metamafic rocks) occur as lenses and dismembered blocks within the anatectic migmatites of the Chencai Group metasedimentary rocks. New SIMS zircon U-Pb dating results show that these mafic rocks underwent high-grade metamorphism at ~427 Ma, similar to that of the metasedimentary rocks. Concordant ages of ~440 Ma for some metamorphic zircon cores suggest that these amphibolites underwent multiple stages of metamorphism during the early Paleozoic orogeny.

2. Zircon O isotope analyses results have $\delta^{18}O$ values scattering around +9 ‰. Most of these metamorphic zircons also possess relatively uniform Lu-Hf isotopic compositions, with calculated $\varepsilon_{Hf}(t)$ values ranging from 9.8 to 15.1. Zircon Hf model ages peak at ~547 Ma, older than the previous result of 496 Ma. We suggest that these newly formed crustal materials were likely extracted from the mantle during the early Paleozoic.

3. The presence of these metamafic rocks might suggest that the previous notion—that a deep lithospheric fracture reaching asthenospheric mantle was absent from the Early Paleozoic South China Orogen—needs to be reconsidered.

ACKNOWLEDGMENTS

Journal editor D. B. Rowley and three reviewers (M. Faure, C. W. Oh, and an anonymous reviewer) are greatly thanked for their very helpful and constructive comments. We are grateful to X. Li, Q. Li, X. Ling, Y. Yang, and C. Li for their help with SIMS zircon U-Pb-O, LA-ICPMS zircon Lu-Hf isotope, and whole-rock Sm-Nd isotope analyses. This work was funded by research programs (grants 41502182, 41530208, 41210003, and 41372196) supported by the National Nature Science Foundation of China, the China Geological Survey (projects 1212010811048 and 12120114064301), the China Postdoctoral Science Foundation (grant 2016T90133), and the China Scholarship Council (file 201604910053).

REFERENCES CITED

Blichert-Toft, J., and Albarède, F. 1997. The Lu-Hf isotope geochemistry of chondrites and the evolution of the mantle-crust system. Earth Planet. Sci. Lett. 148:243–258.

Cawood, P. A.; Wang, Y.; Xu, Y.; and Zhao, G. 2013. Locating South China in Rodinia and Gondwana: a fragment of greater India lithosphere? Geology 41:903–906.

Charvet, J. 2013. The Neoproterozoic–early Paleozoic tectonic evolution of the South China Block: an overview. J. Asian Earth Sci. 74:198–209.

Charvet, J.; Shu, L.; Shi, Y.; Guo, L.; and Faure, M. 1996. The building of South China: collision of Yangzi and Cathaysia blocks, problems and tentative answers. J. Southeast Asian Earth Sci. 13:223–235.

Chen, J.; Foland, K. A.; Xing, F.; Xu, X.; and Zhou, T. 1991. Magmatism along the southeast margin of the Yangtze block: Precambrian collision of the Yangtze and Cathysia blocks of China. Geology 19:815–818.

Chen, X.; Tong, L.; Zhang, C.; Zhu, Q.; and Li, Y. 2015. Retrograde garnet amphibolite from eclogite of the Zhejiang Longyou area: new evidence of the Caledonian orogenic event in the Cathaysia block. Chin. Sci. Bull. 60:1207–1217.

Chen, X.; Zhang Y.; Fan J.; Cheng J.; and Li Q. 2010. Ordovician graptolite-bearing strata in southern Jiangxi with a special reference to the Kwangsian Orogeny. Sci. China Earth Sci. 53:1602–1610.

Chen, X.; Zhang Y.; Fan J.; Tang L.; and Sun H. 2012. Onset of the Kwangsian Orogeny as evidenced by biofacies and lithofacies. Sci. China Earth Sci. 55:1592–1600. doi:10.1007/s11430-012-4490-4.

Corfu, F.; Hanchar, J. M.; Hoskin, P. W. O.; and Kinny, P. 2003. Atlas of zircon textures. Rev. Mineral. Geochem. 53:469–500.

Cui, S., and Li, J. 1983. On the Indosinian movement of China's peri-Pacific tectonic belt. Acta Geol. Sin. 1:51–62 (in Chinese with English abstract).

Faure, M.; Shu, L.; Wang, B.; Charvet, J.; Choulet, F.; and Monie, P. 2009. Intracontinental subduction: a possible mechanism for the early Palaeozoic Orogen of SE China. Terra Nova 21:360–368.

Geisler, T.; Schaltegger, U.; and Tomaschek, F. 2007. Re-equilibration of zircon in aqueous fluids and melts. Elements 3:43–50.

Gerdes, A., and Zeh, A. 2009. Zircon formation versus zircon alteration—new insights from combined U-Pb and Lu-Hf in-situ LA-ICP-MS analyses, and consequences for the interpretation of Archean zircon from the central zone of the Limpopo Belt. Chem. Geol. 261:230–243.

Griffin, W.; Wang, X.; Jackson, S.; Pearson, N.; O'Reilly, S. Y.; Xu, X.; and Zhou, X. 2002. Zircon chemistry and magma mixing, SE China: in-situ analysis of Hf isotopes, Tonglu and Pingtan igneous complexes. Lithos 61:237–269.

Guo, L.; Shi, Y.; Ma, R.; and Dong, H. 1989. The pre-Devonian tectonic patterns and evolution of South China. J. Southeast Asian Earth Sci. 3:87–93.

Guo, L.; Shi, Y.; Ma, R.; Ye, S.; and Lu, H. 1984. Tectonostratigraphic terranes of Southeast China. J. Nanjing Univ. Nat. Sci. Ed. 20:732–739 (in Chinese with English abstract).

He, K.; Nie, Z.; Zhao, C.; Ye, M.; Zhou, Z.; Le, C.; and Tai. D. 2000. Discovering fossils on the late Paleozoic radiolarian in northeast Jiangxi Province. Geosciences 14:1–7, 115–117 (in Chinese with English abstract).

Huang, J. 1941. Chiangnania continent—a Caledonian orogen to the south of Yangtze River. Geol. Rev. 6 (suppl. 2):293–294 (in Chinese).

———. 1960. Preliminary summarization of geologic tectonics in China. Acta Geol. Sin. 40:1–37 (in Chinese).

Jahn, B. M.; Zhou, X. H.; and Li, J. L. 1990. Formation and tectonic evolution of southeastern China and Taiwan: isotopic and geochemical constraints. Tectonophysics 183:145–160.

Kong, X.; Li, Z.; Feng, C.; Gu, G.; and Ma, J. 1995. The Precambrian geology of Chencai region in Zhejiang Province. Beijing, Geological Publishing House (in Chinese).

Li, C.-F.; Li, X.-H.; Li, Q.-L.; Guo, J.-H.; and Li, X.-H. 2011*a*. Directly determining $^{143}Nd/^{144}Nd$ isotope ratios using thermal ionization mass spectrometry for geological samples without separation of Sm-Nd. J. Anal. At. Spectrom. 26:2012–2022.

Li, C.-F.; Li, X.-H., Li, Q.-L.; Guo, J.-H.; Li, X.-H.; and Liu, T. 2011*b*. An evaluation of a single-step extraction chromatography separation method for Sm-Nd isotope analysis of micro-samples of silicate rocks by high-sensitivity thermal ionization mass spectrometry. Anal. Chim. Acta 706:297–304.

Li, J.; Zhang, Y.; Zhao, G.; Johnston, S. T.; Dong, S.; Koppers, A.; Miggins, D. P.; Sun, H.; Wang, W.; and Xin, Y. 2017. New insights into Phanerozoic tectonics of South China: early Paleozoic sinistral and Triassic dextral transpression in the east Wuyishan and Chencai domains, NE Cathaysia. Tectonics 36:819–853.

Li, L.; Lin, S.; Li, J.; He, J.; and Ge, Y. 2018. Zircon U-Pb ages and Hf isotope compositions of the Chencai migmatite, central Zhejiang Province, South China: constraints on the early Palaeozoic orogeny. Geol. Mag. 155:1377–1393.

Li, L.; Lin, S.; Xing, G.; Davis, D. W.; Jiang, Y.; Davis, W.; and Zhang, Y. 2016. Ca. 830 Ma back-arc type volcanic rocks in the eastern part of the Jiangnan orogen: implications for the Neoproterozoic tectonic evolution of South China Block. Precambrian Res. 275:209–224.

Li, Q.-L.; Li, X.-H.; Liu, Y.; Tang, G.-Q.; Yang, J.-H.; and Zhu, W.-G. 2010*a*. Precise U-Pb and Pb-Pb dating of Phanerozoic baddeleyite by SIMS with oxygen flooding technique. J. Anal. At. Spectrom. 25:1107–1113.

Li, S.; Santosh, M.; Zhao, G.; Zhang, G.; and Jin, C. 2012. Intracontinental deformation in a frontier of

super-convergence: a perspective on the tectonic milieu of the South China Block. J. Asian Earth Sci. 49: 313–329.

Li, X.-H. 2000. Geochemistry of the late Paleozoic radiolarian cherts within the NE Jiangxi ophiolite melange and its tectonic significance. Sci. China 43:617–624.

Li, X.-H.; Li, W.-X.; Li, Z.-X.; Lo, C.-H.; Wang, J.; Ye, M.-F.; and Yang, Y.-H. 2009*a*. Amalgamation between the Yangtze and Cathaysia Blocks in South China: constraints from SHRIMP U-Pb zircon ages, geochemistry and Nd-Hf isotopes of the Shuangxiwu volcanic rocks. Precambrian Res. 174:117–128.

Li, X.-H.; Li, Z.-X.; and Li, W.-X. 2014. Detrital zircon U-Pb age and Hf isotope constrains on the generation and reworking of Precambrian continental crust in the Cathaysia Block, South China: a synthesis. Gondwana Res. 25:1202–1215.

Li, X.-H.; Liu, Y.; Li, Q.-L.; Guo, C.-H.; and Chamberlain, K. R. 2009*b*. Precise determination of Phanerozoic zircon Pb/Pb age by multicollector SIMS without external standardization. Geochem. Geophys. Geosyst. 10:Q04010. doi:10.1029/2009GC002400.

Li, X.-H.; Long, W.-G.; Li, Q.-L.; Zheng, Y.-F.; Yang, Y.-H.; Chamberlain, K. R.; Wan, D.-F.; Guo, C.-H.; Wang, X.-C.; and Tao, H. 2010*b*. Penglai zircon megacrysts: a potential new working reference material for microbeam determination of Hf-O isotopes and U-Pb age. Geostand. Geoanal. Res. 34:117–134.

Li, X.-H., and McCulloch, M. T. 1996. Secular variation in the Nd isotopic composition of Neoproterozoic sediments from the southern margin of the Yangtze Block: evidence for a Proterozoic continental collision in southeast China. Precambrian Res. 76:67–76.

Li, X.-H.; Zhao, J.-X.; McCulloch, M. T.; Zhou, G.-Q.; and Xing, F.-M. 1997. Geochemical and Sm-Nd isotopic study of Neoproterozoic ophiolites from southeastern China: petrogenesis and tectonic implications. Precambrian Res. 81:129–144.

Li, Z.-X.; Li, X.-H.; Wartho, J.-A.; Clark, C.; Li, W.-X.; Zhang, C.-L.; and Bao, C. 2010*c*. Magmatic and metamorphic events during the early Paleozoic Wuyi-Yunkai orogeny, southeastern South China: new age constraints and pressure-temperature conditions. Geol. Soc. Am. Bull. 122:772–793.

Li, Z.-X.; Li, X.-H.; Zhou, H.; and Kinny, P. D. 2002. Grenvillian continental collision in south China: new SHRIMP U-Pb zircon results and implications for the configuration of Rodinia. Geology 30:163–166.

Lin, W.; Wang, Q.; and Chen, K. 2008. Phanerozoic tectonics of south China block: new insights from the polyphase deformation in the Yunkai massif. Tectonics 27:TC6004. doi:10.1029/2007TC002207.

Ludwig, K. 2012. User's manual for Isoplot version 3.75–4.15: a geochronological toolkit for Microsoft Excel. Berkeley, CA, Berkeley Geochronological Center.

Manton, R. J.; Buckman, S.; Nutman, A. P.; Bennett, V. C.; and Belousova, E. A. 2017. U-Pb-Hf-REE-Ti zircon and REE garnet geochemistry of the Cambrian Attunga eclogite, New England Orogen, Australia: implications for continental growth along eastern Gondwana. Tectonics 36:1580–1613.

Mao, J.; Takahashi, Y.; Kee, W.-S.; Li, Z.; Ye, H.; Zhao, X.; Liu, K.; and Zhou, J. 2011. Characteristics and geodynamic evolution of Indosinian magmatism in South China: a case study of the Guikeng pluton. Lithos 127:535–551.

Miyashiro, A. 1961. Evolution of metamorphic belts. J. Petrol. 2:277–311.

Ren, J. 1964. Preliminary investigations on the several issues about the tectonics of the pre-Devonian southeast China. Acta Geol. Sin. 44:418–431, 489 (in Chinese with Russian abstract).

Ren, J., and Chen, T. 1989. Tectonic evolution of the continental lithosphere in eastern China and adjacent areas. J. Southeast Asian Earth Sci. 3:17–27.

Ren, J.; Chen, T.; Liu, Z.; Niu, B.; and Liu, F. 1986. Some problems on the tectonics of South China. Chin. Sci. Bull. 31:751–754.

Ren, J., and Li, C. 2016. Cathaysia Old Land and relevant problems: pre-Devonian tectonics of southern China. Acta Geol. Sin. 90:607–614 (in Chinese with English abstract).

Ren, J.; Niu, B.; and Liu, Z. 1999. Soft collision, superposition orogeny and polycyclic suturing. Earth Sci. Front. 6:85–93 (in Chinese with English abstract).

Rubatto, D., and Gebauer, D. 1996. Use of cathodoluminescence for U-Pb zircon dating by ion microprobe: some examples from the Western Alps. *In* Pagel, M.; Barbin, V.; Blanc, P.; and Ohnenstetter, D., eds. Cathodoluminescence in geosciences. Berlin, Springer, p. 373–400.

Rubatto, D.; Gebauer, D.; and Compagnoni, R. 1999. Dating of eclogite-facies zircons: the age of Alpine metamorphism in the Sesia-Lanzo Zone (Western Alps). Earth Planet. Sci. Lett. 167:141–158.

Shu, L. S. 2012. An analysis of principal features of tectonic evolution in South China Block. Geol. Bull. China 31:1035–1053 (in Chinese with English abstract).

Shu, L. S.; Jahn, B. M.; Charvet, J.; Santosh, M.; Wang, B.; Xu, X. S.; and Jiang, S. Y. 2014. Early Paleozoic depositional environment and intraplate tectono-magmatism in the Cathaysia Block (South China): evidence from stratigraphic, structural, geochemical and geochronological investigations. Am. J. Sci. 314:154–186.

Shu, L. S.; Zhou, G.-O.; and Shi, Y.-S. 1994. Study of the high pressure metamorphic blueschist and its late Proterozoic age in the eastern Jiangnan belt. Chin. Sci. Bull. 39:1200–1204.

Sláma, J.; Košler, J.; Condon, D. J.; Crowley, J. L.; Gerdes, A.; Hanchar, J. M.; Horstwood, M. S.; Morris, G. A.; Nasdala, L.; and Norberg, N. 2008. Plešovice zircon—a new natural reference material for U-Pb and Hf isotopic microanalysis. Chem. Geol. 249:1–35.

Söderlund, U.; Patchett, P. J.; Vervoort, J. D.; and Isachsen, C. E. 2004. The ^{176}Lu decay constant determined by Lu-Hf and U-Pb isotope systematics of Precambrian mafic intrusions. Earth Planet. Sci. Lett. 219:311–324.

Spear, F. S. 1995. Metamorphic phase equilibria and pressure-temperature-time paths. Washington, DC, Mineralogical Society of America.

Stacey, J. S., and Kramers, J. D. 1975. Approximation of terrestrial lead isotope evolution by a two-stage model. Earth Planet. Sci. Lett. 26:207–221.

Valley, J. W. 2003. Oxygen isotopes in zircon. Rev. Mineral. Geochem. 53:343–385.

Valley, J. W.; Kinny, P. D.; Schulze, D. J.; and Spicuzza, M. J. 1998. Zircon megacrysts from kimberlite: oxygen isotope variability among mantle melts. Contrib. Mineral. Petrol. 133:1–11.

Vavra, G., and Hansen, B. T. 1991. Cathodoluminescence studies and U/Pb dating of zircons in pre-Mesozoic gneisses of the Tauern Window: implications for the Penninic basement evolution. Geol. Rundsch. 80:703–715.

Vavra, G.; Schmid, R.; and Gebauer, D. 1999. Internal morphology, habit and U-Th-Pb microanalysis of amphibolite-to-granulite facies zircons: geochronology of the Ivrea Zone (Southern Alps). Contrib. Mineral. Petrol. 134:380–404.

Wang, J.-G.; Yu, S.-Q.; Hu, Y.-H.; Zhao, X.-D.; Wu, M.; and Gu, M.-G. 2014*a*. The discovery, petrology and geochronology of the retrograde eclogite in Jiangshan-Shaoxing suture zone. Geol. China 41:1356–1363 (in Chinese with English abstract).

Wang, J. Q.; Shu, L. S.; and Yu, J. H. 2016. Petrological properties and tectonic significance for Longyou garnet amphibolite. Chin. Sci. Bull. 61:125–134.

———. 2017. From the Neoproterozoic mafic rock to the Silurian high-grade metamorphic rock: evidence from zircon U-Pb geochronological, bulk-rock geochemical and mineral EPMA studies of Longyou garnet amphibolite in SE China. J. Asian Earth Sci. 141:7–23.

Wang, X.-L.; Shu, L.-S.; Xing, G.-F.; Zhou, J.-C.; Tang, M.; Shu, X.-J.; Qi, L.; and Hu, Y.-H. 2012*a*. Post-orogenic extension in the eastern part of the Jiangnan orogen: evidence from *ca* 800–760 Ma volcanic rocks. Precambrian Res. 222–223:404–423.

Wang, X.-L.; Zhao, G.; Zhou, J.-C.; Liu, Y.; and Hu, J. 2008. Geochronology and Hf isotopes of zircon from volcanic rocks of the Shuangqiaoshan Group, South China: implications for the Neoproterozoic tectonic evolution of the eastern Jiangnan orogen. Gondwana Res. 14:355–367.

Wang, X.-L.; Zhou, J.-C.; Griffin, W. L.; Zhao, G.; Yu, J.-H.; Qiu, J.-S.; Zhang, Y.-J.; and Xing, G.-F. 2014*b*. Geochemical zonation across a Neoproterozoic orogenic belt: isotopic evidence from granitoids and metasedimentary rocks of the Jiangnan orogen, China. Precambrian Res. 242:154–171.

Wang, Y.; Fan, W.; Zhang, G.; and Zhang, Y. 2013*a*. Phanerozoic tectonics of the South China Block: key observations and controversies. Gondwana Res. 23: 1273–1305.

Wang, Y.; Wu, C.; Zhang, A.; Fan, W.; Zhang, Y.; Zhang, Y.; Peng, T.; and Yin, C. 2012*b*. Kwangsian and Indosinian reworking of the eastern South China Block: constraints on zircon U-Pb geochronology and metamorphism of amphibolites and granulites. Lithos 150: 227–242.

Wang, Y.; Zhang, A.; Fan, W.; Zhang, Y.; and Zhang, Y. 2013*b*. Origin of paleosubduction-modified mantle for Silurian gabbro in the Cathaysia Block: geochronological and geochemical evidence. Lithos 160-161:37–54.

Wang, Y.; Zhang, F.; Fan, W.; Zhang, G.; Chen, S.; Cawood, P. A.; and Zhang, A. 2010. Tectonic setting of the South China Block in the early Paleozoic: resolving intracontinental and ocean closure models from detrital zircon U-Pb geochronology. Tectonics 29:TC6020. doi:10.1029/2010TC002750.

Wasserburg, G.; Jacobsen, S.; DePaolo, D.; McCulloch, M.; and Wen, T. 1981. Precise determination of Sm/Nd ratios, Sm and Nd isotopic abundances in standard solutions. Geochim. Cosmochim. Acta 45:2311–2323.

Wong, W. H. 1929. The Mesozoic orogenic movement in eastern China. Bull. Geol. Soc. China 8:33–44.

Woodhead, J. D., and Hergt, J. M. 2005. A preliminary appraisal of seven natural zircon reference materials for in situ Hf isotope determination. Geostand. Geoanal. Res. 29:183–195.

Wu, F.; Sun, J.; and Zhang, X. 1998. The Nd isotopic evidence for late Paleozoic oceanic crust in southern margin of Yangtze block. Acta Petrol. Sin. 14:23–33 (in Chinese with English abstract).

Wu, F.-Y.; Yang, Y. H.; Xie, L. W.; Yang, J. H.; and Xu, P. 2006. Hf isotopic compositions of the standard zircons and baddeleyites used in U-Pb geochronology. Chem. Geol. 234:105–126.

Xie, L.; Zhang, Y.; Zhang, H.; Sun, J.; and Wu, F. 2008. In situ simultaneous determination of trace elements, U-Pb and Lu-Hf isotopes in zircon and baddeleyite. Chin. Sci. Bull. 53:1565–1573.

Xing, G.; Li, L.; Jiang, Y.; Feng, Y.; Lu, Q.; Chen, Z.; Yu, M.; and Duan, Z. 2014. Petrogenetic process of Cretaceous "gneissic" magma-mixed complex in the Changle-Nan'ao structure zone, Fujian Province: a case study on Xiaocun intrusion. Resour. Surv. Environ. 35:79–94 (in Chinese with English abstract).

Xing, G.; Lu, Q.; Jiang, Y.; Nie, T.; Chen, R.; Feng, Y.; Chen, Z.; et al. 2010. Identification and significance of "gneissic" magma-mixed complex in the Changle-Nan'ao fault zone, southeastern Fujian, China. Geol. Bull. China 29:31–43 (in Chinese with English abstract).

Xu, X.; Xue, D.; Li, Y.; Hu, P.; and Chen, N. 2014. Neoproterozoic sequences along the Dexing-Huangshan fault zone in the eastern Jiangnan orogen, South China: geochronological and geochemical constrains. Gondwana Res. 25:368–382.

Yang, S.; Chen, H.; Wu, G.; and Dong, C. 1995. Discovery of early Paleozoic island-arc volcanic rock in northern part of Fujian Province and the significance for tectonic study. Sci. Geol. Sin. 30:105–116 (in Chinese with English abstract).

Yang, Y.-H.; Zhang, H.-F.; Chu, Z.-Y.; Xie, L.-W.; and Wu, F.-Y. 2010. Combined chemical separation of Lu, Hf, Rb, Sr, Sm and Nd from a single rock digest and precise and accurate isotope determinations of Lu-Hf, Rb-Sr and Sm-Nd isotope systems using multi-collector ICP-MS and TIMS. Int. J. Mass Spectrom. 290:120–126.

Yao, J.; Shu, L.; Cawood, P. A.; and Li, J. 2016. Delineating and characterizing the boundary of the Cathaysia Block and the Jiangnan orogenic belt in South China. Precambrian Res. 275:265–277.

Yao, J.; Shu, L.; Santosh, M.; and Xu, Z. 2014. Palaeozoic metamorphism of the Neoproterozoic basement in NE Cathaysia: zircon U-Pb ages, Hf isotope and whole-rock geochemistry from the Chencai Group. J. Geol. Soc. Lond. 171:281–297.

Yao, W.-H.; Li, Z.-X.; Li, W.-X.; Wang, X.-C.; Li, X.-H.; and Yang, J.-H. 2012. Post-kinematic lithospheric delamination of the Wuyi-Yunkai orogen in South China: evidence from ca. 435 Ma high-Mg basalts. Lithos 154:115–129.

Yin, H.; Wu, S.; Du, Y.; and Peng, Y. 1999. South China defined as part of Tethyan archipelagic ocean system. Earth Sci. 24:3–14 (in Chinese with English abstract).

Yu, J.; Lou, F.; Wang, L.; Shen, L.; Zhou, X.; Zhang, C.; and Huang, Z. 2014. The geological significance of a Paleozoic mafic granulite found in the Yiyang area of northeastern Jiangxi Province. Chin. Sci. Bull. (Chinese ed.) 59:3508–3516.

Zeh, A.; Gerdes, A.; Klemd, R.; and Barton, J. M. 2007. Archaean to Proterozoic crustal evolution in the central zone of the Limpopo belt (South Africa–Botswana): constraints from combined U-Pb and Lu-Hf isotope analyses of zircon. J. Petrol. 48:1605–1639.

Zhang, C.-L.; Santosh, M.; Zhu, Q.-B.; Chen, X.-Y.; and Huang, W.-C. 2015*a*. The Gondwana connection of South China: evidence from monazite and zircon geochronology in the Cathaysia Block. Gondwana Res. 28:1137–1151.

Zhang, C.-L.; Santosh, M.; Zou, H.-B.; Li, H.-K.; and Huang, W.-C. 2013*a*. The Fuchuan ophiolite in Jiangnan Orogen: geochemistry, zircon U-Pb geochronology, Hf isotope and implications for the Neoproterozoic assembly of South China. Lithos 179:263–274.

Zhang, C.-L.; Zhu, Q.-B.; Chen, X.-Y.; and Ye, H.-M. 2016. Ordovician arc-related mafic intrusions in South China: implications for plate subduction along the southeastern margin of South China in the early Paleozoic. J. Geol. 124:743–767.

Zhang, G.; Guo, A.; Wang, Y.; Li, S.; Dong, Y.; Liu, S.; He, D.; Cheng, S.; Lu, R.; and Yao, A. 2013*b*. Tectonics of South China continent and its implications. Sci. China Earth Sci. 56:1804–1828.

Zhang, K.-J. 2017. A Mediterranean-style model for early Neoproterozoic amalgamation of South China. J. Geodyn. 105:1–10.

Zhang, Y., and Wang, Y. 2016. Early Neoproterozoic (~840 Ma) arc magmatism: geochronological and geochemical constraints on the metabasites in the Central Jiangnan Orogen. Precambrian Res. 275:1–17.

Zhang, Y.; Wang, Y.; Zhang, Y.; and Zhang, A. 2015*b*. Neoproterozoic assembly of the Yangtze and Cathaysia blocks: evidence from the Cangshuipu Group and associated rocks along the Central Jiangnan Orogen, South China. Precambrian Res. 269:18–30.

Zhao, C.; He, K.; Mo, X.; Tai, D.; Ye, D.; Ye, N.; Lin, P.; Bi, X.; Zheng, B.; and Feng, Q. 1996. Discovery and its significance of late Paleozoic radiolarian silicalite in ophiolitic melange of northeastern Jiangxi deep fault belt. Chin. Sci. Bull. 41:667–670.

Zhao, G. 2014. Jiangnan Orogen in South China: developing from divergent double subduction. Gondwana Res. 27:1173–1180.

Zhao, L.; Li, T.; Peng, P.; Guo, J.; Wang, W.; Wang, H.; Santosh, M.; and Zhai, M. 2015*a*. Anatomy of zircon growth in high pressure granulites: SIMS U-Pb geochronology and Lu-Hf isotopes from the Jiaobei Terrane, eastern North China Craton. Gondwana Res. 28:1373–1390.

Zhao, L.; Zhai, M.; Santosh, M.; and Zhou, X. 2017. Early Mesozoic retrograded eclogite and mafic granulite from the Badu Complex of the Cathaysia Block, South China: petrology and tectonic implications. Gondwana Res. 42:84–103.

Zhao, L.; Zhai, M.; Zhou, X.; Santosh, M.; and Ma, X. 2015*b*. Geochronology and geochemistry of a suite of mafic rocks in Chencai area, South China: implications for petrogenesis and tectonic setting. Lithos 236–237:226–244.

———. 2016. Thermal gradient and geochronology of a Paleozoic high-grade terrane in the northeastern Cathaysia block, South China. Tectonophysics 691:311–327.

Zhao, L.; Zhou, X.; Zhai, M.; Santosh, M.; and Geng, Y. 2015*c*. Zircon U-Th–Pb-Hf isotopes of the basement rocks in northeastern Cathaysia block, South China: implications for Phanerozoic multiple metamorphic reworking of a Paleoproterozoic terrane. Gondwana Res. 28:246–261.